Karlsruhe Institute of Technology

Wave phenomena
analysis and numerics

# Second-harmonic bichromatic dispersive wave comb generation in a dissipative Kerr temporal soliton Fabry-Perot

Lukas Bengel, Francesco R. Talenti, Ahmedreza Alaeddini, Carolin Scheib, Björn de Rijk, Wolfgang Reichel, Guiseppe Leo, Christian Koos, Huanfa Peng, Stefan Wabnitz

CRC Preprint 2025/55, December 2025

KARLSRUHE INSTITUTE OF TECHNOLOGY

CRC 1173

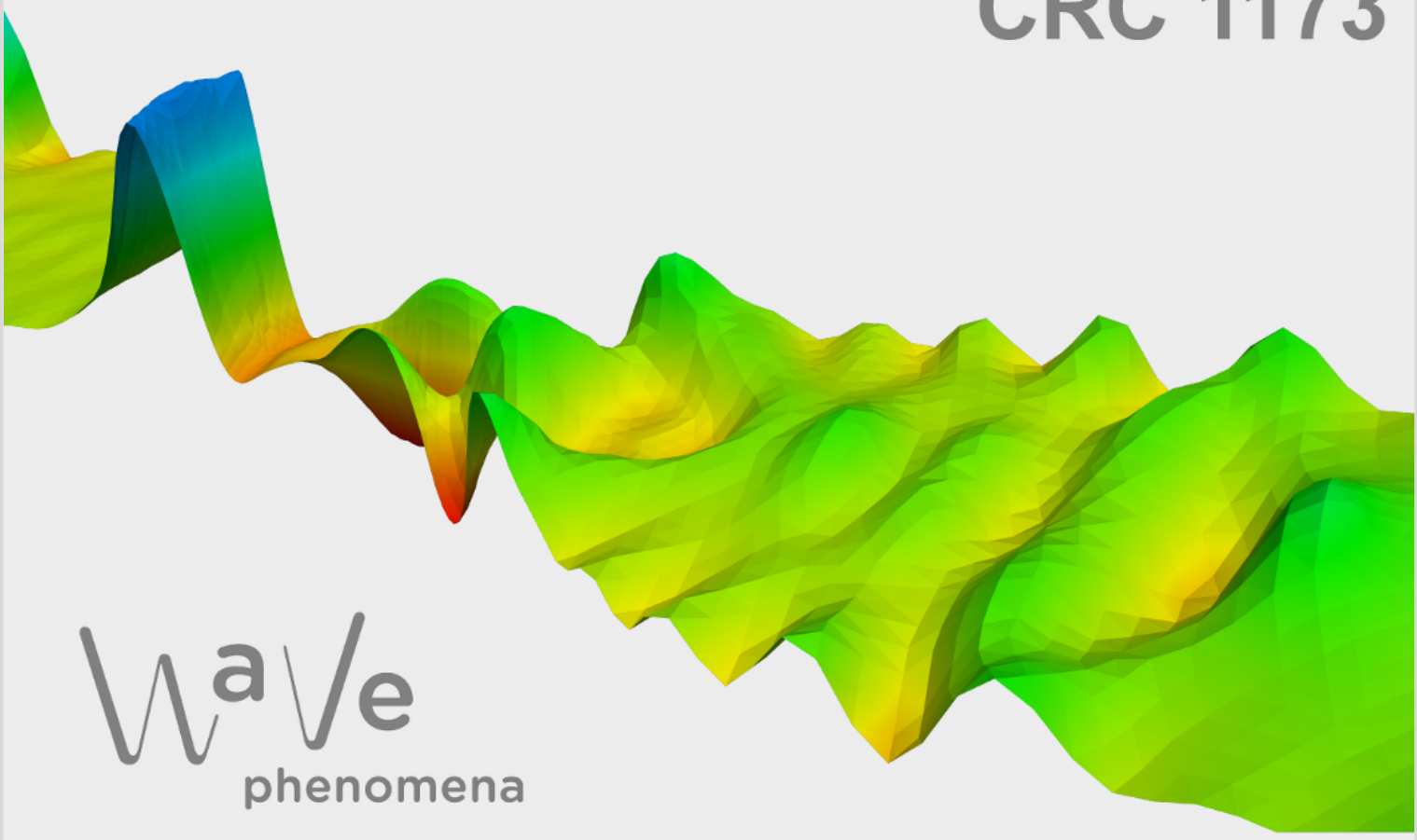

**Participating universities**





**Funded by**


ISSN 2365-662X

# Second-Harmonic Bichromatic Dispersive Wave Comb Generation in a Dissipative Kerr Temporal Soliton Fabry-Perot

LUKAS BENGEL[1], FRANCESCO RINALDO TALENTI[2,3], AHMEDREZA ALAEDDINI[4], CAROLIN SCHEIB[5], BJÖRN DE RIJK[1], WOLFGANG REICHEL[1], GIUSEPPE LEO[3,6], CHRISTIAN KOOS[5], HUANFA PENG[5], AND STEFAN WABNITZ[4,7]

[1] *Department of Mathematics, Karlsruhe Institute of Technology (KIT), 76131 Karlsruhe, Germany*
[2] *Université Paris-Saclay, CNRS, Centre for Nanosciences and Nanotechnology, 91120 Palaiseau, France*
[3] *Laboratoire Matériaux et Phénomènes Quantiques (MPQ), Université Paris Cité, 75205 Paris, France*
[4] *DIET, Sapienza University of Rome, Via Eudossiana, 00184 Roma, Italy*
[5] *Institute of Photonics and Quantum Electronics (IPQ), Karlsruhe Institute of Technology (KIT), 76131 Karlsruhe, Germany*
[6] *Institut Universitaire de France, France*
[7] *CNR-INO, Istituto Nazionale di Ottica, Via Campi Flegrei 34, 80078 Pozzuoli, Italy*
[*] *stefan.wabnitz@uniroma1.it*

*Compiled December 21, 2025*

**We introduce a novel example of space-time analogy, where a dissipative soliton microcomb generates a traveling-wave temporal Fabry-Perot for trapping a bichromatic dispersive comb, generated at the second-harmonic of the pump laser. The fundamental frequency comb is generated in the anomalous dispersion regime, whereas the dispersive comb is generated in the normal dispersion regime. Direct numerical simulations are in excellent agreement with an analytical model.**

In recent years, there has been significant research interest in the study of optical pulse propagation in spatiotemporal dispersive media. We are considering here the novel effects that may arise in the presence of a refractive index modulation, both in space and time, which is induced by a traveling-wave perturbation. In this context, intriguing space-time analogies, such as temporal reflection and refraction, total internal reflection, and temporal guiding from a moving boundary have been revealed [1]. For example, an optical fiber soliton permits to introduce, via cross-phase-modulation, a traveling-wave refractive index perturbation which acts on a weak dispersive wave propagating at a different wavelength [2, 3]. Moreover, the propagation of either a soliton pair or a soliton train provides the temporal analog of a waveguide or a Fabry–Perot resonator [4, 5] or a spatiotemporal moving Bragg grating mirror [6].

In this work, we introduce a new example of a wave propagation effect that can be explained in terms of space-time analogies. Specifically, we show that dissipative (or cavity) Kerr solitons (DKS) associated with a coherent frequency comb in the anomalous dispersion regime of a microresonator may create a Fabry-Perot resonator temporal cavity for dispersive waves at different carrier frequencies. In the relevant case where the microresonator has both quadratic and cubic nonlinearities, a time-stationary dispersive wave is spontaneously generated by the fundamental frequency (FF) soliton comb via phase-matched intra-cavity second-harmonic (SH) generation. Based on numerical experiments, we show that the usual sweeping of the frequency detuning of the FF coherently injected CW laser across the cavity resonance leads to the simultaneous generation of a stable pair of coupled combs, comprising a FF soliton comb and a dispersive SH comb.

Along with that, recent experimental demonstrations of two-colors comb generation [7, 8] motivate deeper theoretical investigations of nonlinear cavity systems with simultaneous $\chi^{(2)}$ and $\chi^{(3)}$ nonlinearities [9–11]. In these systems, combs may result from a strong nonlinear interaction of both types of nonlinearities. Here we consider a different situation, where the properties of the SH comb generated in the normal dispersion regime are determined by the linear temporal waveguides, which are dynamically induced via cross-phase modulation by the train of DKS at the FF in the anomalous dispersion regime.

Let us consider the set of coherently driven and damped mean-field equations that describe propagation in a passive cavity with both quadratic and cubic nonlinearities [9, 10, 12–14]:

$$\begin{cases} \dfrac{\partial A}{\partial t} = \left[-\alpha_1 - i\Delta - i\eta_1 \dfrac{\partial^2}{\partial \tau^2}\right] A + i\kappa B A^* + S \\ \qquad + \left[i\gamma_1 |A|^2 + 2i\gamma_{12}|B|^2\right] A \qquad (1) \\ \dfrac{\partial B}{\partial t} = \left[-\alpha_2 - i2\Delta - d\dfrac{\partial}{\partial \tau} - i\eta_2 \dfrac{\partial^2}{\partial \tau^2}\right] B + i\kappa A^2 \\ \qquad + \left[i\gamma_2 |B|^2 + i2\gamma_{21}|A|^2\right] B \quad . \qquad (2) \end{cases}$$

Here $A$ and $B$ are the wave amplitudes at the FF (index 1) and the SH (index 2), respectively. The CW laser source $S$ coherently

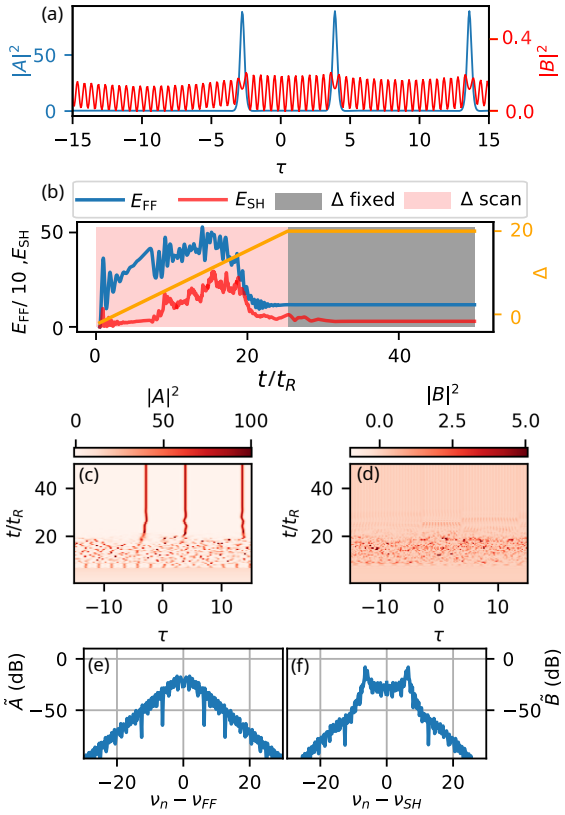


**Fig. 1.** (a) Temporal profile of a FF cavity soliton coupled to a dispersive SH wave. (b) Intracavity energy of the FF and SH field while sweeping the detuning Δ. (c-d) Temporal evolution of the FF and SH fields. (e-f) Final spectrum for the field $A$ and $B$. The values used for this simulation are $\alpha_{1,2} = 1$, $\eta_1 = -1$, $\eta_2 = 1$, $\kappa = 0.5$, $\gamma_{1,12} = 0.5$, $\gamma_{2,21} = 1$, $S = 12$, $t_R = 30$ , $d = 0$.

drives the passive cavity with distributed losses ($\alpha_{1,2}$), with a laser/cavity detuning (Δ), group-velocity walk-off ($d$) and group velocity dispersion (GVD) ($\eta_{1,2}$). The quadratic nonlinear coefficient is $\kappa$, whereas the self-phase ($\gamma_{1,2}$) or cross-phase ($\gamma_{12,21}$) modulation terms are associated with the cubic nonlinearity of the cavity. For simplicity, Eqs. (1-2) are written for the case of phase-matched SH generation.

Following [9], we numerically simulated the generation of coupled $\chi^{(2)} + \chi^{(3)}$ combs by using Eqs. (1-2). As it is typically done in experiments for the generation of DKS combs, we introduced a linear ramp of the pump laser-cavity detuning Δ over the first 25 round-trips (from $\Delta = -2$ up to $\Delta = 20$); we kept Δ fixed for the subsequent 25 round trips to test the stability of the numerically excited intracavity field solutions. For the moment, let us consider the case of a vanishing linear group-velocity walk-off between the FF and the SH, i.e., we set $d = 0$ in Eqs. (1-2). However, in contrast with the case studied in [9], which investigates anomalous dispersion for both fields, we now consider a FF (SH) propagating in the anomalous (normal) GVD regime, respectively.

The final state (Fig. 1(a)) in the temporal profile of the intracavity intensity is very different for the FF and the SH. Three DKSs per round-trip are formed at the FF. Whereas, a synchronous dispersive wave with fast oscillating intensity, which is trapped between the DKSs, forms at the SH. The intensity of the SH dispersive wave is reduced by more than two orders of magnitude with respect to the DKS at the FF. Observing the intracavity energy build-up (computed as the fast time integrals of $|A|^2$ and $|B|^2$, Fig. 1(b)), it is evident that most of the energy is carried by the FF wave. The dynamics results in the typical generation of a Kerr DKS emerging from a chaotic spatiotemporal evolution (see panel (c)). Around the SH, though, the relatively low energy state does not allow the formation of a localized solution (panel (d)).

In Fig. 1(e-f) we report the final spectra for both the FF and SH waves, respectively. Once the DKS comb is established at the FF, a symmetric double-peaked comb is generated around the SH. Interestingly, the dominant spectral component of the SH wave slightly mismatches its nominal central frequency $\nu_{SH}$. This result may suggest a dynamical oscillatory behavior which requires an attentive analysis.

In order to understand what determines the temporal frequency of the SH comb, we perform a loop of numerical simulations by sweeping the value of $\eta_2$, while keeping all other parameters constant. While increasing $\eta_2$, the oscillation frequency $k_*$ of the SH wave diminishes. This is evident by looking at both the temporal (Fig. 2(a-b)) and spectral (Fig. 2(c)) profiles. In panel (d) we show how $k_*$ strictly depends on dispersive effects and it decreases with the inverse square root of $\eta_2$. Because of the much reduced intensity of the SH comb, it is expected that its properties can be described in terms of a linearized model. As we are going to confirm by an approximate but analytical solution of this model, the temporal period of the oscillation of the field intensity at the SH remains fixed all across the round-trip time. Moreover, below we present a simple explicit formula for $k_*$ which matches our numerical experiments as shown in Fig. 2(d).

To systematically study the standing- and traveling-wave solutions of Eqs. (1-2) observed in the direct numerical simulations, one sets $A(t,\tau) = a(\tau - ct)$, and $B(t,\tau) = b(\tau - ct)$. This leads to a system of ordinary differential equations for the wave

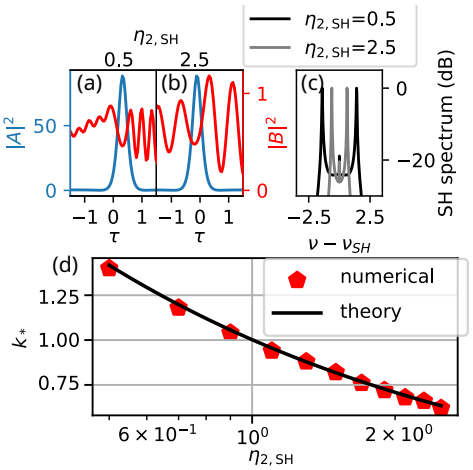


**Fig. 2.** (a-b) temporal profiles of the FF and SH field for two different values of $\eta_{2,SH} = 0.5$ and 2.5, respectively, and (c) their associated spectra. (d) Comparison between the numerical simulations and theory. Other simulation parameters are: $\alpha_{1,2} = 1$, $\eta_1 = -1$, $\kappa = 1$, $\gamma_{1,12} = 0.5$, $\gamma_{2,21} = 1$, $S = 12$, $t_R = 50$ , $d = 0$.

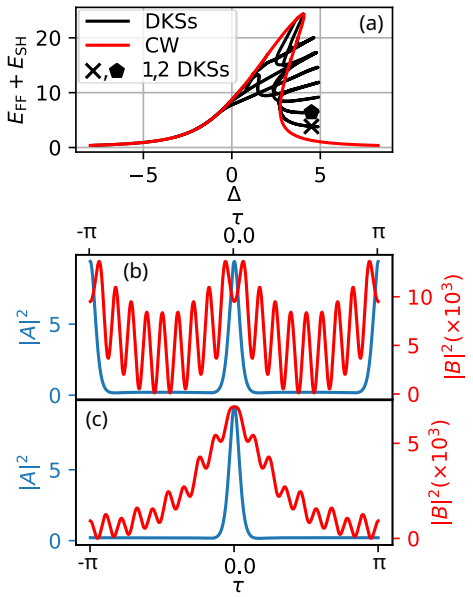


**Fig. 3.** (a) Bifurcation diagram for Eq. (1-2). In red, we report the CW solution connected with the black branches consisting of coupled combs. (b-c) Temporal profiles of the two solutions indicated in panel (a) corresponding to one and two DKSs in the FF field. The values of the parameters are $\alpha_{1,2} = 1$, $\eta_1 = -0.1$, $\eta_2 = 0.1$, $\kappa = 0.1$, $\gamma_{1,12,21,2} = 1$, $S = 2$, $t_R = 2\pi$, $d = 0$.

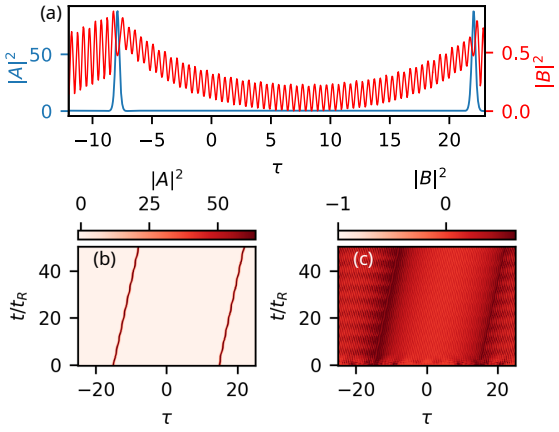


**Fig. 4.** (a) Zoom on the temporal profiles of two drifting FF solitons coupled to a SH dispersive wave with $\eta_2$=1 (normal dispersion) and group-velocity walk-off $d = 1.5$. (b-c) The associated FF and SH dynamics. Other simulation parameters are: $\alpha_{1,2} = 1$, $\eta_1 = -1$, $\eta_2 = 1$, $\kappa = 1$, $\gamma_{1,12} = 0.5$, $\gamma_{2,21} = 1$, $S = 12$, $t_R = 50$.

profiles $a, b$, where the wave speed $c$ is part of the unknowns. For this system, we performed a numerical bifurcation analysis using the MATLAB package `pde2path` [15], which is designed to treat systems of coupled differential equations. Choosing the detuning Δ as the bifurcation parameter, we computed the curve of steady-state solutions of Eqs. (1-2), along with the bifurcation points on this curve. Retaining the assumption of zero walk-off, the system is reversible in $\tau$, i.e., invariant with respect to the transformation $\tau \mapsto -\tau$. Thus, we may find bifurcations of symmetric coupled standing-wave solutions with $c = 0$. In Fig. 3 panel (a) we report the bifurcation diagram, and in panels (b) and (c) we show the coupled combs that bifurcate from the steady-state solution of Eqs. (1-2), in the case when either only one or two DKSs are present in each round-trip time of the FF comb. States with three DKSs per round-trip, such as those shown in Fig. 1(a), emerge from the third bifurcation branch in Fig. 3(a). The steady-state solutions exhibit, in the presence of multiple DKSs per round-trip, a much larger amplitude of the oscillations of the SH intracavity field; cf. Fig. 3(b-c).

Next, we numerically investigated the robustness of the dynamical $\omega \rightleftarrows 2\omega$ interplay in the presence of a nonzero group-velocity walk-off $d$. Fig. 4(a) shows two FF DKSs coupled to a dispersive SH wave for a finite walk-off ($d = 1.5$). Panels (b–c) illustrate the corresponding FF and SH temporal dynamics: when $d \neq 0$, the solitons undergo a drift, yet the overall $\omega \rightleftarrows 2\omega$ coupling remains qualitatively unchanged. This observation is consistent with the numerical bifurcation analysis, as for $d \neq 0$, traveling-wave solutions with $c \neq 0$ emerge near Hopf bifurcations. Quantitatively, the resulting bifurcation diagrams are almost identical to the $d = 0$ case displayed in Fig. 3(a), since the walk-off primarily affects the weak SH field, and has a negligible impact on the total intracavity energy $E_{FF} + E_{SH}$. For this reason, we decided not to display the corresponding bifurcation diagrams. To analyze the effect of the walk-off on the coupled combs in more detail, we performed a path continuation in $d$ using the solution displayed in Fig. 3(c) as the starting point. We first observe in Fig. 5(a) that the dominant SH frequencies $\pm k_*$ undergo a symmetry breaking into asymmetrically spaced frequencies $k_\pm$. This symmetry breaking occurs in both the temporal and the spectral profiles displayed in Fig. 5, and it is explained by the fact that for $d \neq 0$ the system loses reversibility in $\tau$.

In Fig. 5(b) we report the solution branch parametrized by $d$ but we only display the energy of the SH field, which decreases after a few oscillations; the energy of the FF field remains nearly constant along the branch. Panels (c-h) of Fig. 5 show the gradual change of the temporal and spectral profiles of the traveling coupled comb and the SH field, respectively. For $d = 1$ (panels (c-d)), the negative carrier frequency slightly approaches the CW component, while its positive counterpart loses energy and moves towards higher frequency. This trend is confirmed for $d = 10$ (panels (e-f)) and $d = 20$ (panels (g-h)). Finally, we note that Fig. 5 shows that, as $d$ increases, the dispersive wave in the SH field undergoes a smooth transition toward a waveform similar to a dark pulse.

In order to obtain better theoretical insight in the properties of the dispersive wave comb, we now derive a simple analytical model for the SH field. When neglecting the self-phase-modulation term for the weak SH field, one obtains the linear equation for $B$:

$$\left[\alpha_2 + 2i\Delta + d\frac{\partial}{\partial\tau} + i\eta_2\frac{\partial^2}{\partial\tau^2}\right] B - 2i\gamma_{21}|A|^2 B = i\kappa A^2. \quad \textbf{(3)}$$

Let us assume now that the FF field forms a localized DKS, which can be approximated by the formula $A \simeq A_1 \mathrm{sech}(A_2\tau) - iS/\Delta$, where the amplitude is $|A_1| = \sqrt{2\Delta}$ and $A_2 = \sqrt{-\Delta/\eta_1} > 0$ (see [16, 17]). Applying the discrete Fourier transform, denoted by $(\cdot)^\sim$, for $2\pi$-periodic functions to Eq. (3) yields

$$\left[\alpha_2 + 2i\Delta + idk - i\eta_2 k^2 - 2i\gamma_{21}\frac{S^2}{\Delta^2}\right] B_k = \left[i\kappa A^2 + 2i\gamma_{21}(|A|^2 - \frac{S^2}{\Delta^2})B\right]^{\sim}(k). \quad \textbf{(4)}$$

Here, $B_k = \tilde{B}(k)$ denotes the $k$-th Fourier mode of the SH field. Since we consider a localized DKS at the FF field, its spectral envelope is locally flat when subtracting the CW contribution. This means that the spectrum of $|A|^2 - S^2/\Delta^2$ decays slowly in $|k|$. Consequently, the right-hand side of Eq. (4) is almost locally constant in $k$, with the exception of the 0-th Fourier mode, which typically dominates the spectrum due to the strong 0-th spectral component of $A^2$ caused by the CW pump. We deduce that the SH field has dominant Fourier modes $B \simeq B_{k_\pm} e^{ik_\pm \tau}$, where $k_\pm$ minimizes the modulus of the Fourier multiplier

$$\alpha_2 + 2i\Delta + idk - i\eta_2 k^2 - 2i\gamma_{21}\frac{S^2}{\Delta^2}. \quad \textbf{(5)}$$

The real part of (5) equals the distributed loss $\alpha_2$ which is independent of $k$. Thus, equating the imaginary part of (5) to 0, we readily obtain the explicit expressions

$$k_\pm = \frac{d \pm \sqrt{d^2 + 8\eta_2\Delta - 8\eta_2\gamma_{21}\frac{S^2}{\Delta^2}}}{2\eta_2}. \quad \textbf{(6)}$$

This indicates the presence of two spectral peaks in the SH field at the frequencies $k_\pm$, which are clearly discernible in our numerical simulations; see Fig. 1(f) and Fig. 5(d,f,h). Since the distributed loss $\alpha_2$ equals the minimal modulus of the Fourier multiplier (5), one naturally expects that these peaks become increasingly pronounced as $\alpha_2$ tends to 0. When $d = 0$, system (1-2) is reversible in $\tau$, resulting in symmetric spectra; see Fig. 1(e-f). Consequently, $B_k = B_{-k}$ and the dominant Fourier mode is $B \simeq B_{k_*} cos(k_*\tau)$, where $k_* = k_+ = -k_-$. Fig. 2(d) shows an excellent agreement between theory, as predicted by Eq. (6), and results of direct numerical simulations for $d = 0$. Notably, the observation that $k_*$ decreases with the inverse square root of $\eta_2$ for $d = 0$ is confirmed by Eq. (6). Furthermore, Eq. (6) implies that $k_-$ tends to 0 as $d \to \infty$, while $k_+$ diverges to $\infty$, which is consistent with the findings in Fig. 5. In particular, Fig. 5(a) shows that Eq. (6) yields accurate predictions for the positions of spectral peaks for increasing values of $d$.

In conclusion, we propose a novel space-time analogy, predicting a temporal Fabry-Perot formed by a dominant Kerr dynamics coupled towards a dispersive second harmonic wave. The $\omega \rightleftarrows 2\omega$ interaction produces a second-harmonic wave that becomes trapped between the mirrored solitons formed around the pump wavelength, with its oscillatory behavior tightly governed by dispersion. We observe a spectral symmetry breaking by considering a non-zero walk-off, which connects double peaked spectra to standard dark solitons solutions. Our findings open the path towards a novel class of octave-spanning comb generation sources based on promising material platforms such as AlGaAs-on-insulator [18].

**Funding.** ANR-22-CE92-0065, DFG-505515860 (Quadcomb); EU - NRRP, NextGenerationEU (PE00000001 - program "RESTART"), Deutsche Forschungsgemeinschaft (DFG, German Research Foundation) – Project-ID 258734477 – SFB 1173.

**Disclosures.** The authors declare no conflicts of interest.

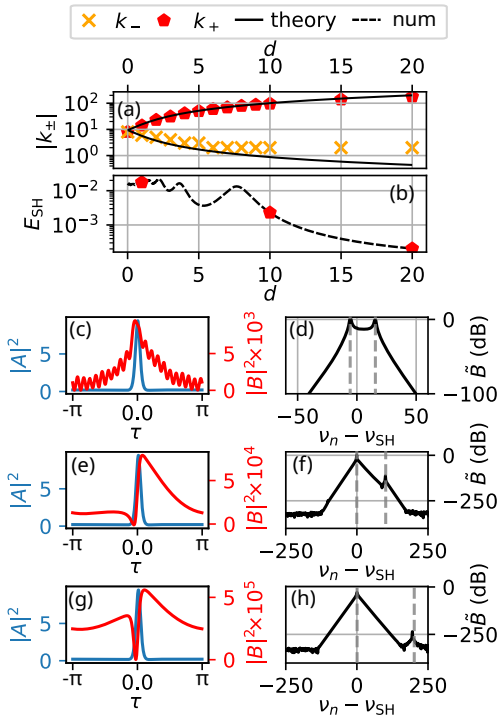


**Fig. 5.** Continuation of the coupled comb of Fig. 3 (c) in $d$. (a) Comparison between theory (solid lines) and numerics of the dominant frequency components. (b) Numerical computation of the intracavity energy of the SH field for increasing values of $d$; red dots refer to the cases of panels (c-h). (c-h) Temporal profiles of the traveling FF and SH field with the spectral profiles of the SH field for $d = 1, 10, 20$. The dashed lines in panels (c-h) display the values of $k_\pm$ according to Eq. (6).

## REFERENCES

1. G. P. Agrawal, J. Opt. **27**, 043003 (2025).
2. A. Demircan, S. Amiranashvili, and G. Steinmeyer, Phys. Rev. Lett. **106**, 163901 (2011).
3. T. G. Philbin, C. Kuklewicz, S. Robertson, *et al.*, Science **319**, 1367 (2008).
4. S. Wang, A. Mussot, M. Conforti, *et al.*, Opt. Lett. **40**, 3320 (2015).
5. J. Zhang, W. Donaldson, and G. P. Agrawal, J. Opt. Soc. Am. B **38**, 2376 (2021).
6. J. Zhang, W. R. Donaldson, and G. P. Agrawal, Opt. Lett. **49**, 5854 (2024).
7. A. W. Bruch, X. Liu, Z. Gong, *et al.*, Nat. Photonics **15**, 21 (2021).
8. J. Lu, D. N. Puzyrev, V. V. Pankratov, *et al.*, Nat. Commun. **14**, 2798 (2023).
9. F. R. Talenti, S. Wabnitz, Y. Sun, *et al.*, Opt. Lett. **50**, 2037 (2025).
10. G. Wu, Y. Wei, L. Li, *et al.*, Phys. Rev. Lett. **135**, 113801 (2025).
11. M. Shi, N. Englebert, F. Leo, *et al.*, Phys. Rev. A **112**, 023522 (2025).
12. F. Leo, T. Hansson, I. Ricciardi, *et al.*, Phys. Rev. A **93**, 043831 (2016).
13. T. Hansson, P. Parra-Rivas, M. Bernard, *et al.*, Opt. Lett. **43**, 6033 (2018).
14. X. Xue, F. Leo, Y. Xuan, *et al.*, Light. Sci. & Appl. **6**, e16253 (2017).
15. H. Uecker, D. Wetzel, and J. D. M. Rademacher, Numer. Math. Theory Methods Appl. **7**, 58 (2014).
16. S. Wabnitz, Opt. Lett. **18**, 601 (1993).
17. L. Bengel and B. de Rijk, Phys. D: Nonlinear Phenom. **483**, 134922 (2025).
18. F. R. Talenti, L. Lovisolo, A. Gerini, *et al.*, J. Eur. Opt. Soc. Publ. **21**, 23 (2025).

## FULL REFERENCES


1. G. P. Agrawal, "Propagation of optical pulses in a spatiotemporal dispersive medium," J. Opt. **27**, 043003 (2025).
2. A. Demircan, S. Amiranashvili, and G. Steinmeyer, "Controlling light by light with an optical event horizon," Phys. Rev. Lett. **106**, 163901 (2011).
3. T. G. Philbin, C. Kuklewicz, S. Robertson, *et al.*, "Fiber-optical analog of the event horizon," Science **319**, 1367–1370 (2008).
4. S. Wang, A. Mussot, M. Conforti, *et al.*, "Bouncing of a dispersive wave in a solitonic cage," Opt. Lett. **40**, 3320–3323 (2015).
5. J. Zhang, W. Donaldson, and G. P. Agrawal, "Time-domain fabry–perot resonators formed inside a dispersive medium," J. Opt. Soc. Am. B **38**, 2376–2382 (2021).
6. J. Zhang, W. R. Donaldson, and G. P. Agrawal, "Spatiotemporal bragg gratings forming inside a nonlinear dispersive medium," Opt. Lett. **49**, 5854–5857 (2024).
7. A. W. Bruch, X. Liu, Z. Gong, *et al.*, "Pockels soliton microcomb," Nat. Photonics **15**, 21 (2021).
8. J. Lu, D. N. Puzyrev, V. V. Pankratov, *et al.*, "Two-colour dissipative solitons and breathers in microresonator second-harmonic generation," Nat. Commun. **14**, 2798 (2023).
9. F. R. Talenti, S. Wabnitz, Y. Sun, *et al.*, "Bistable soliton optical frequency combs in a second-harmonic generation kerr cavity," Opt. Lett. **50**, 2037–2040 (2025).
10. G. Wu, Y. Wei, L. Li, *et al.*, "Ultraflat soliton microcombs in driven quadratic-kerr nonlinear microresonators," Phys. Rev. Lett. **135**, 113801 (2025).
11. M. Shi, N. Englebert, F. Leo, *et al.*, "Modulation instability and frequency-comb generation in hybrid quadratic-cubic resonators with spectral filtering," Phys. Rev. A **112**, 023522 (2025).
12. F. Leo, T. Hansson, I. Ricciardi, *et al.*, "Frequency-comb formation in doubly resonant second-harmonic generation," Phys. Rev. A **93**, 043831 (2016).
13. T. Hansson, P. Parra-Rivas, M. Bernard, *et al.*, "Quadratic soliton combs in doubly resonant second-harmonic generation," Opt. Lett. **43**, 6033–6036 (2018).
14. X. Xue, F. Leo, Y. Xuan, *et al.*, "Second-harmonic-assisted four-wave mixing in chip-based microresonator frequency comb generation," Light. Sci. & Appl. **6**, e16253–e16253 (2017).
15. H. Uecker, D. Wetzel, and J. D. M. Rademacher, "pde2path—a Matlab package for continuation and bifurcation in 2D elliptic systems," Numer. Math. Theory Methods Appl. **7**, 58–106 (2014).
16. S. Wabnitz, "Suppression of interactions in a phase-locked soliton optical memory," Opt. Lett. **18**, 601–603 (1993).
17. L. Bengel and B. de Rijk, "Existence and stability of soliton-based frequency combs in the Lugiato–Lefever equation," Phys. D: Nonlinear Phenom. **483**, 134922 (2025).
18. F. R. Talenti, L. Lovisolo, A. Gerini, *et al.*, "Interplay of $\chi$ (2) and $\chi$ (3) effects for microcomb generation," J. Eur. Opt. Soc. Publ. **21**, 23 (2025).